



**ONLINE FIRST (NOT Peer-Reviewed)**

Title: Enhancement of photoelectrocatalysis efficiency of carbon nanotubes doped with TiO<sub>2</sub> nanostructures applied on pesticide degradation

Received: 2019-02-11

Online First: 2019-02-25

Process: I. First trial (Field and check)



II. Peer review



III. Editing and three trials



IV. Published online



PiscoMed Publishing Pte. Ltd. Singapore



# Enhancement of photoelectrocatalysis efficiency of carbon nanotubes doped with TiO<sub>2</sub> nanostructures applied on pesticide degradation

## ABSTRACT

In this study, a composite electrode based on multi-walled carbon nanotubes (MWCNT) and titanium dioxide (TiO<sub>2</sub>) prepared by the sol-gel method was synthesized and evaluated for the photoelectrochemical oxidation of carbaryl. The MWCNT/TiO<sub>2</sub> composite was deposited into a titanium plate (Ti) and characterised by scanning electron microscopy (SEM), X-ray diffraction (XRD), and electrochemically. The photoelectrochemical oxidation of carbaryl was studied to evaluate potential applications of the Ti/MWCNT/TiO<sub>2</sub> composite electrode in environmental science. The carbaryl removal efficiency yielded 71.0% at an applied potential of +1.5 V for 1 h using the Ti/MWCNT/TiO<sub>2</sub> composite electrode in presence of light. In comparison, the removal efficiency reached 57.6% using the same parameters, however in absence of light. The results demonstrated the interesting photoelectrochemical properties of the developed material when applied on the pesticide degradation.

**Keywords:** Carbon nanotubes, Titanium dioxide, Carbaryl

## Introduction

The titanium dioxide (TiO<sub>2</sub>) has displayed to be one of the most excellent photocatalyst material owing to its strong oxidation activity, chemical stability, nontoxicity, low-cost fabrication, and economic efficiency for the oxidative decomposition of many organic compounds [1-2]. The TiO<sub>2</sub> can be synthesized by various methods like sol-gel, hydrothermal, electro-spinning, chemical vapor deposition or by the combination of these methods, forming different morphologies such as nanoparticle, nanorods, nanotubes, nanoflowers, and nanofibers [3-5].

The coupling of carbon nanotubes (CNTs) and TiO<sub>2</sub> has attracted much attention in the literature. The CNTs have some beneficial effects on the photocatalytic activity of TiO<sub>2</sub> by inducing synergies or cooperative effects between the metal oxide and carbon phases [6-8]. Some works have emphasized the preparation of CNTs-TiO<sub>2</sub> composite materials and their application in many fields such as photoelectrocatalysis [9] and photocatalytic activity [10] of methylene blue degradation, hydrogen generation [1] and oxidation of some pollutants in aqueous [12-14] and gaseous phase [15]. Nevertheless no work has been found about the use of the CNTs-TiO<sub>2</sub> composite in the photoelectro-oxidation of the carbaryl pesticide, which is widely used as an insecticide throughout the world. In the other side, several works has been reported about the electrochemical degradation of carbaryl using different dimensionally stable anodes. Gelover *et al.* [16] proposed a solar detoxification of carbaryl in water using films of TiO<sub>2</sub> supported over small glass cylinders and Pramauro *et al.* [17] used TiO<sub>2</sub> dispersions irradiated with simulated solar light to the photocatalytic degradation of carbaryl in aqueous.

Considering that which has been described above, this study focuses on the synthesis and characterization of a composite based on multi-walled carbon nanotube (MWCNT) and titanium



oxides prepared by the sol-gel method. The MWCNT/TiO<sub>2</sub> composite was deposited on a titanium surface by dip-coating and annealing techniques. The novel composite formed was evaluated for the degradation of carbaryl in aqueous solutions.

## 2. Experimental

### 2.1. Chemicals and solutions

All chemicals were of analytical grade and were used without further purification. Analytical-grade carbaryl, isopropanol, and titanium (IV) tetraisopropoxide [Ti(C<sub>3</sub>H<sub>6</sub>OH)<sub>4</sub>, 97%], were purchased from Sigma-Aldrich (Germany). Phosphate buffer solution (PBS) was used as a supporting electrolyte with ionic strength at 0.1 mol L<sup>-1</sup>. All solutions were prepared with water purified in a Millipore Milli-Q system (resistivity > 18.2 MΩ cm). Multi-walled carbon nanotubes (MWCNT - purity of 95%, length 5–15 μm, diameter 50–100 nm) was obtained from Sigma-Aldrich. The MWCNT were previously functionalized following the work proposed by Moraes et al. [18]. For this, 1.0 g of MWCNTs was mixed

with 500 mL of a 1:3 mixture of HNO<sub>3</sub>/H<sub>2</sub>SO<sub>4</sub> for 12 hours. This was then filtered through a 0.45 μm Millipore Nylon<sup>®</sup> filter membrane. The resulting MWCNT was continuously washed using distilled water until the pH of the filtrate was neutral, and then dried overnight in a vacuum oven at 120 °C.

### 2.2. Procedures

Photoelectrochemical experiments were carried out in a photocell with a quartz window (d= 2.5 cm). Photocurrent behavior was carried out using a linear sweep voltammetry (LSV) in 0.1 mol L<sup>-1</sup> of Na<sub>2</sub>SO<sub>4</sub> solution as electrolyte. A solar simulator (Newport Oriel Arc lamp housing 67005, Oriel xenon lamp 6255, Oriel Arc lamp power supply 69907 USA) was used as light source. Differential pulse voltammetry (DPV) and chronoamperometry (CA) experiments were performed using a PGSTAT 302 Autolab electrochemical system (Eco Chemie, Netherlands) monitored with NOVA software. The electrochemical cell was assembled with a conventional three-electrode system: A

titanium plate modified with a MWCNT/TiO<sub>2</sub> as a working electrode, an Ag/AgCl electrode in KCl (3.0 mol L<sup>-1</sup>) as a reference electrode, and a Pt wire as an auxiliary electrode. All electrochemical measurements were performed in 0.1 mol L<sup>-1</sup> PBS (pH 6.0) containing 100.0 μmol L<sup>-1</sup> of carbaryl standard, at controlled temperature (25 °C). DPV curves were obtained in a potential range from +0.8 to +2.0 V with a scan rate of 5 mV s<sup>-1</sup>, amplitude at 100 mV, and step potential of 2 mV. The carbaryl electrolysis experiment was performed using CA at a fixed potential of +1.5 V for one hour, monitored using UV-visible spectrophotometer Jasco V-630 at 220 nm.

The band gap energy ( $E_g$ ) to MWCNT/TiO<sub>2</sub> composite was calculated from UV-vis diffuse reflectance spectroscopy (DRS) carried in Cary 5 E spectrometer (Agilent Technologies) with the wavelength operating from 200 to 800 nm

The field-emission gun scanning electron microscopy (FEG-SEM) images were recorded using a FEG-Zeiss model Supra 35 VP (Zeiss, Germany). The structural characterization was performed by X-ray diffraction (XRD) using a Rigaku Rotaflex Diffractometer model RU200B at 50 kV and 100 mA, with a Cu Kα radiation wavelength of  $\lambda = 1.542$  Å. Diffuse reflectance spectra were obtained using a UV-vis-NIR spectrometer (Perkin Elmer Lambda 35).

### 2.3. Synthesis of the MWCNT/TiO<sub>2</sub>

The MWCNT/TiO<sub>2</sub> films were prepared using the sol-gel and dip-coating methods based on the work proposed Sánchez and Rincón [19]. The sol-gel was obtained mixing 100 mg of MWCNT previously functionalized, 40.0 mL of isopropanol and acidify with HCl. The mixture was kept under stirring conditions. Thus 1.5 mL of titanium (IV) tetraisopropoxide (TTIP) was slowly added in the MWCNT suspension. The system was kept under stirring at 60° C in order to the gel formation. A previously cleaned, polished and smoothed titanium plate was dipped into the sol-gel and placed in an oven

at 400°C for 5 min, after each dipping-withdrawing process. The dip-coated films were submitted to 25 dipping-withdrawing-annealing cycles, before being sintered at 400 °C for 60 min as the final step.

## 3. Results and discussion

### 3.1. Morphological and structural characterization of the MWCNT/TiO<sub>2</sub>

The morphological characterization of the MWCNT/TiO<sub>2</sub> was evaluated using FEG-SEM microscopy. Figure 1 display typical images of MWCNT and the composite assembled over titanium plate electrodes. In Figure 1A it can be observed that the MWCNT were dispersed over the Ti substrate. Also the MWCNT presented an average radius at 80 nm with a length close to 1.0 µm. After the synthesis the obtained composite was showed in Figure 1B, in which, it can be observed that the TiO<sub>2</sub> presented a more compact microstructures with large particles of length close to 4 µm. However, observing the Figure 1B inset it can be noted that the also are formed some fleck-like small particles of the titanium oxides In order to evaluate the crystalline phases of the MWCNT/TiO<sub>2</sub> nanoparticles, XRD patterns were obtained. In Figure 2, it was possible to observe that the diffraction peaks are a combined response of CNTs and of TiO<sub>2</sub>. The presence of TiO<sub>2</sub>nanoparticles in the composite was characterized by the appearance of diffraction peaks in special at 25.4°, 37.8°, and 70.2°, which can be readily indexed anatase phase. The brookite peaks, usually observed for TiO<sub>2</sub> obtained from sol gel method, can be not found in this case [20]. The XRD data of the MWCNT/TiO<sub>2</sub> presented a typical carbon reflection peak (002) at 26.2°, which can be attributed to the graphitic phase of the carbon nanotubes. The hexagonal phase (012) of the CNTs appeared at 42.3° and 44.5°. There are also six peaks that can be indexed to the metallic titanium (substrate) that appeared at 35.1°, 38.5°, 40.1°, 53.1°, 62.9° and 70.7°. XRD results were also analyzed using the Scherrer equation [21] in order to estimate the mean crystallite size of the composite. The estimated mean crystallite size was 18.6 nm for the TiO<sub>2</sub>, with a lattice strain at 0.979%, which is according results observed by Carrera-Lopez and Castillo Cervantes [20].

### 3.2. electrochemical characterization of the MWCNT/TiO<sub>2</sub>

The photoelectrochemical behaviour of the MWCNT/TiO<sub>2</sub> composite was evaluated using diffuse reflectance and LSV under illumination and chronoamperometry upon

light on/off measurements. The band-gap ( $E_g$ ) was estimated using the Wood-Tauc equation [22], i.e.  $(\alpha h\nu)^s = h\nu - E_g$ , in which,  $\alpha$  is the absorption coefficient,  $h\nu$  is the photon energy and  $E_g$  is the band-gap energy. The  $E_g$  value is estimated by the extrapolation of the linear section of the plot  $(\alpha h\nu)^s$  vs.  $h\nu$ , as displayed in Figure 3A and 3B for TiO<sub>2</sub> and MWCNT/TiO<sub>2</sub> films, respectively.

Following Freitas et al. [23], the value used for  $s$  was fixed at 0.5, once the TiO<sub>2</sub>anatase



phase could be classified as an indirect gap semiconductor. Thus, straight-line portion of the curve, when extrapolated to zero, gives the optical band gap ( $E_g$ ) that was estimated at 3.19 eV for  $\text{TiO}_2$  and 2.4 to  $\text{MWCNT}/\text{TiO}_2$  composites. This band-gap value is in agreement of other works that reported the band-gap value for anatase close to 3.20 eV [24]. As observed different authors, the inclusion of MWCNT induces the increased light absorption intensity in the visible region [25-27].

The photoelectrochemical activity of the  $\text{MWCNT}/\text{TiO}_2$  composite was evaluated based on a water splitting reaction, in which the system photocurrent was measured by LSV. Figure 4 shows the typical photocurrent versus the measured potential for  $\text{MWCNT}/\text{TiO}_2$  composite electrodes under illumination. The results are also shown for the DPV for one of the samples under dark conditions. It was clear to observe that, under illumination the  $\text{MWCNT}/\text{TiO}_2$  composite electrodes exhibited a huge increase in the anodic current, almost 3.5-fold, compared with the system in absence of light. This behavior is due the  $\text{TiO}_2$  a n-type semiconductor. In presence of a light source the excitons are generate in the semiconductor. The electrons of valence band are promoted to conduct band and the holes ( $h_{vb}^+$ ) are created in the semiconductor surface. As observed in the Figure 4 inset, under illumination, the electrons are photogenerated at the  $\text{TiO}_2$  nanoparticles with concomitant transport to the  $\text{MWCNT}/\text{GC}$  substrate producing a photocurrent. Switching off the light, the recombination between electrons from the  $\text{TiO}_2$  conduction band and holes decreases the photocurrent.

It was evident  $\text{MWCNT}/\text{TiO}_2$  composite electrodes exhibited an interesting photoelectrochemical behavior, that can be used as photoanode on carbaryl oxidation. In this sense, a possible mechanism of the pesticide oxidation could be based on semiconductor-mediated photodegradation initiated by the surface electron injection (denoted as SMPD) [28]. Based on the  $\text{TiO}_2$  light-induced water splitting experiment the  $\text{TiO}_2$  acts as a good oxidation catalyst for oxygen evolution because of the particularly low overvoltage (closed to +0.2 V) [29,30]. Thus, in the presence of visible light, the  $\text{TiO}_2$  could adsorb energy larger than the band gap of the semiconductor, exciting electrons from the valence band to the conduction band. The band-band excitation produces the reductive conduction band electrons ( $e_{cb}^-$ ) and oxidative band holes ( $h_{vb}^+$ ). The holes can react with surface-adsorbed  $\text{H}_2\text{O}$ , producing a hydroxyl radicals ( $\bullet\text{OH}$  – equation 1).

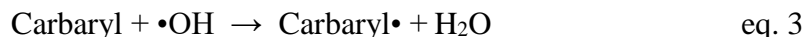


In presence of oxygenated media, the  $e_{cb}^-$  electrons are usually scavenged by  $\text{O}_2$  to yield superoxide radical anions ( $\bullet\text{O}_2^-$  - equation 2).



Based on the carbaryl electrochemical oxidation profile over the  $\text{MWCNT}/\text{TiO}_2$  surface, as displayed in the voltammograms of Figure 5, the electrode was polarized at +1.5 V,

i.e. after the carbaryl oxidation peak. In this potential values, the hydroxyl radicals ( $\bullet\text{OH}$ ) could be oxidizing the carbaryl in two paths, as demonstrated in equations 3 and 4, respectively. First, the pesticide reacts with  $\bullet\text{OH}$ , forming another radical specie (carbaryl $\bullet$ ). Subsequently, the carbaryl $\bullet$  reacts with  $\text{O}_2$ , leading to a degradation product.



In this case, the excess of charge in the depletion zone of the TiO<sub>2</sub> semiconductor added promotes the formation of hydroxyl radicals from water splitting allowing the electro-oxidation of the pesticide. In addition, when the chemical and electrochemical steps were performed, a large increase in the oxidation current peak was observed that could lead to an effective system of pesticide degradation.

### 3.3. Optimisation of the MWCNT/TiO<sub>2</sub> synthesis for the oxidation of carbaryl

The influence of the MWCNT/TiO<sub>2</sub> composite synthesis for the oxidation of carbaryl was studied using DPV in the potential interval of +0.8 to +2.0 V vs. Ag/AgCl/KCl (3.0 mol L<sup>-1</sup>) and in a 0.1 mol L<sup>-1</sup> PBS pH 6.0 containing 100.0 μmol L<sup>-1</sup> of carbaryl. Accordingly, three main parameters were studied, these being, the amount of TTIP, the number of dipping-withdrawing-annealing cycles and the time that the Ti/MWCNT/TiO<sub>2</sub> composite was sintered as shown in Table 1.

First, the TTIP volume was optimised in the range of 0.5 to 2.0 mL, with fixed quantity of MWCNT. The voltammetric profiles had peaks at almost identical potentials of approximately +1.25 V for all TTIP composition studied. The peak current values for carbaryl oxidation increased up to 1.5 mL of TTIP and decrease when more than 1.5 mL of TTIP was used in the composite preparation. This occurs because when minor TTI quantities are added in the synthesis, the MWCNT are more exposed on the material surface and are not totally assembled inside the small titanium oxides structures. Based on these results, 1.5 mL of TTIP was used in the composite synthesis.

Another parameter studied, was the number of dipping-withdrawing-annealing cycles, varying in the range of 5 to 30 times, that the Ti/MWCNT/TiO<sub>2</sub> composite was submitted. The highest peak current for the carbaryl oxidation was observed when the dip-coated films were subjected to 25 dipping-withdrawing-annealing cycles, remained practically constant above this value. Therefore, 25 dipping-withdrawing-annealing cycles was used in the next experiments.

Finally, the time in which the Ti/MWCNT/TiO<sub>2</sub> composite was sintered at 400 °C was

also optimized. For this, the oven time was varied from 1 to 6 hours. It was not observed variation on the peak current for the carbaryl oxidation. Thus, the Ti/MWCNT/TiO<sub>2</sub> composite was sintered for one hour at 400 °C as final step.

### 3.4. The carbaryl electrochemical and photoelectrochemical degradation study

In order to evaluate the effect of the Ti/MWCNT/TiO<sub>2</sub> composite on the carbaryl electrochemical and photoelectrochemical oxidation, chronoamperometric studies monitored with UV-vis were performed. Based on the oxidation process observed on the DPV experiments, the chronoamperometry studies were carried out at +1.5 V during 60 minutes, in 0.1 mol L<sup>-1</sup> of PBS pH 6.0 containing 50.0 μmol L<sup>-1</sup> of carbaryl. The electrolysis experiments were monitored using UV-vis absorption measurements at 220 nm. This wavelength is due to the maximum values of the carbaryl molar absorptivity ( $\epsilon = 82696 \text{ L mol}^{-1} \text{ cm}^{-1}$ ) [31].



The Figure 6 shows the percentage of the carbaryl degradation as a function of the time, during the electrolysis step for the following electrodes: Ti plate (curve a), Ti/MWCNT (curve b) and Ti/MWCNT/TiO<sub>2</sub> (curve c). It was observed that in the three electrodes studied the carbaryl concentration decreased. The Ti plate electrode exhibited a lower percentage of decrease, i.e. only 25.4% of the initial concentration. For the Ti electrode modified with MWCNT sol-gel the initial concentration decreased 35.5%. However, the Ti/MWCNT/TiO<sub>2</sub> composite electrode yielded a decrease of 57.6%. Using the Lambert-Beer law the final concentration of carbaryl was calculated at 21.2 μmol L<sup>-1</sup>. These results showed that the MWCNT/TiO<sub>2</sub> composite electrode becomes a promising setup for electrochemical degradation of carbaryl, degrading more than 2.0-fold of the carbaryl pesticide, when compared with bare Ti and 1.6-fold compared with Ti/MWCNT electrode.

Also in Figure 6, the photoelectrochemical activity of the MWCNT/TiO<sub>2</sub> composite electrode on the carbaryl degradation is presented. For this purpose, the chronoamperometry studies were performed in the presence of light (curve d) using the same parameters described above. As expected, the results showed that when the electrolysis was performed under illumination, the MWCNT/TiO<sub>2</sub> composite electrode exhibited an increased in the percentage of degradation, being the degradation of the carbaryl 1.3 times higher compared with the experiments performed in the absence of light using the same electrode (curve c). The percentage of degradation in relation of the initial concentration of carbaryl was 71.0%, demonstrating the photoelectrochemical properties of the MWCNT/TiO<sub>2</sub> composite electrode when applied on the pesticide degradation.

#### **4. Conclusion**

A composite based on MWCNT and TiO<sub>2</sub> prepared by the sol-gel method was synthesized and successfully characterised by XRD, SEM, and electrochemical techniques. The characterisations indicated that the CNT were covered by small particles of the titanium oxides structures, in which the TiO<sub>2</sub> presented a mean crystallite size of 18.62 nm. The photoelectrochemical properties of the MWCNT/TiO<sub>2</sub> composite showed greater efficiency in the degradation of carbaryl achieving 71.0% of removal.

In essence, the Ti/MWCNT/TiO<sub>2</sub> composite electrode can be an effective anodic material for carbaryl degradation and presents itself as an alternative material to be used in environmental analysis.

#### **Acknowledgements**

We are grateful for financial support from FAPESP (grant 2017/24274-3).

#### **References**



**Tables**

**Table 1.** Optimized parameters of the MWCNT/TiO<sub>2</sub> composite synthesis for the oxidation of carbaryl in DPV

<b>Parameter</b>	<b>Optimized value</b>
Volume of TTIP	1.5 mL
Number of dipping-withdrawing-annealing cycles	25 cycles
Oven time at 400 °C	1 hour



## Figure caption

**Figure 1.** FEG-SEM micrographs for: (A) MWCNT and (B) MWVNT/TiO<sub>2</sub> composite.

**Figure 2.** XRD patterns of MWVNT/TiO<sub>2</sub> composite over Ti substrate. The peaks labelled correspond to: (—) TiO<sub>2</sub> anatase, (—) carbon and (—) Ti metallic.

Figure 3. b Diffuse reflectance data plot  $(ah\nu)^{0.5}$  versus photon energy  $(h\nu)$  for: (A) TiO<sub>2</sub> and (B) MWVNT/TiO<sub>2</sub> composite.

**Figure 4.** Linear sweep voltammograms, at 25 mV s<sup>-1</sup>, obtained for MWVNT/TiO<sub>2</sub> composite electrode in 0.1 mol L<sup>-1</sup> 0.1 mol L<sup>-1</sup> of PBS (pH 6.0) in: (○) absence of light and (○) presence of solar simulated illumination. Inset: photocurrent response MWVNT/TiO<sub>2</sub> composite to ON/OFF cycles of light illumination.

**Figure 5.** Differential pulse voltammograms of the MWVNT/TiO<sub>2</sub> composite electrode in 0.1 mol L<sup>-1</sup> PBS (pH 6.0) containing 100.0 μmol L<sup>-1</sup> of carbaryl standard, with a scan rate of 5 mV s<sup>-1</sup>, amplitude at 100 mV, and step potential of 2 mV. Inset: proposed electrochemical mechanism for carbaryl oxidation.

**Figure 6.** Electrochemical and photoelectrochemical oxidation of carbaryl for the three different electrodes: Ti plate (curve a), Ti/MWCNT (curve b) and Ti/MWCNT/TiO<sub>2</sub> in the absence (curve c) and in the presence of light (curve d). The experiments were carried out at +1.5 V in 0.1 mol L<sup>-1</sup> of PBS pH 6.0 containing 50.0 μmol L<sup>-1</sup> of carbaryl, monitored using UV-vis absorption measurements at 220 nm.

Figure 1. Cesarino, I. et al.

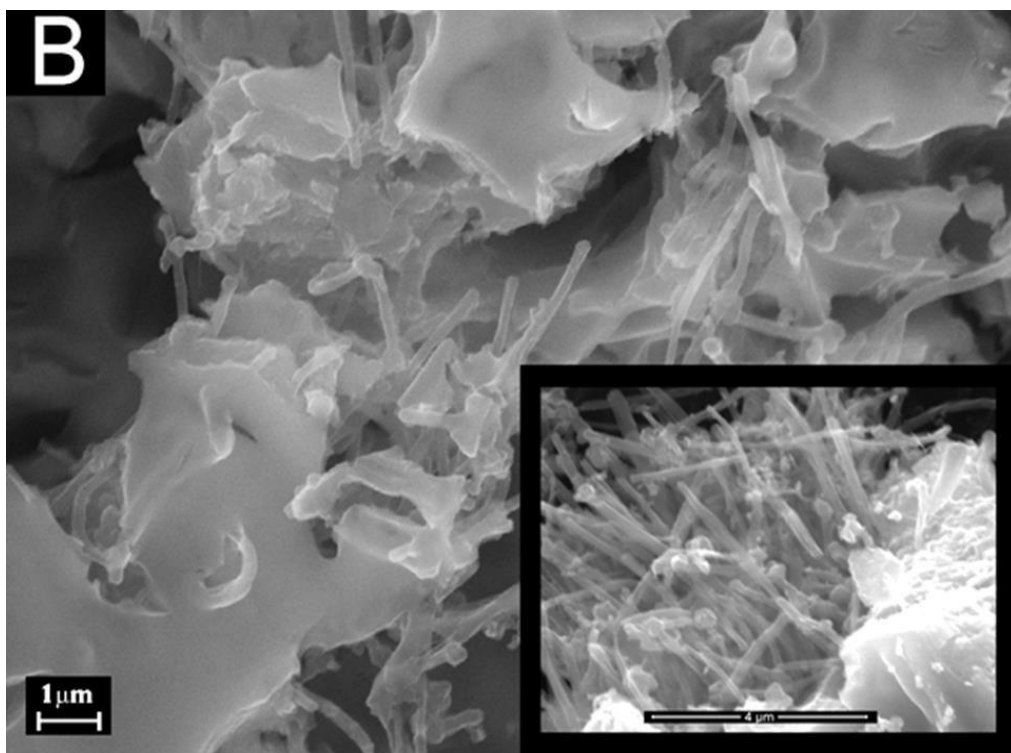
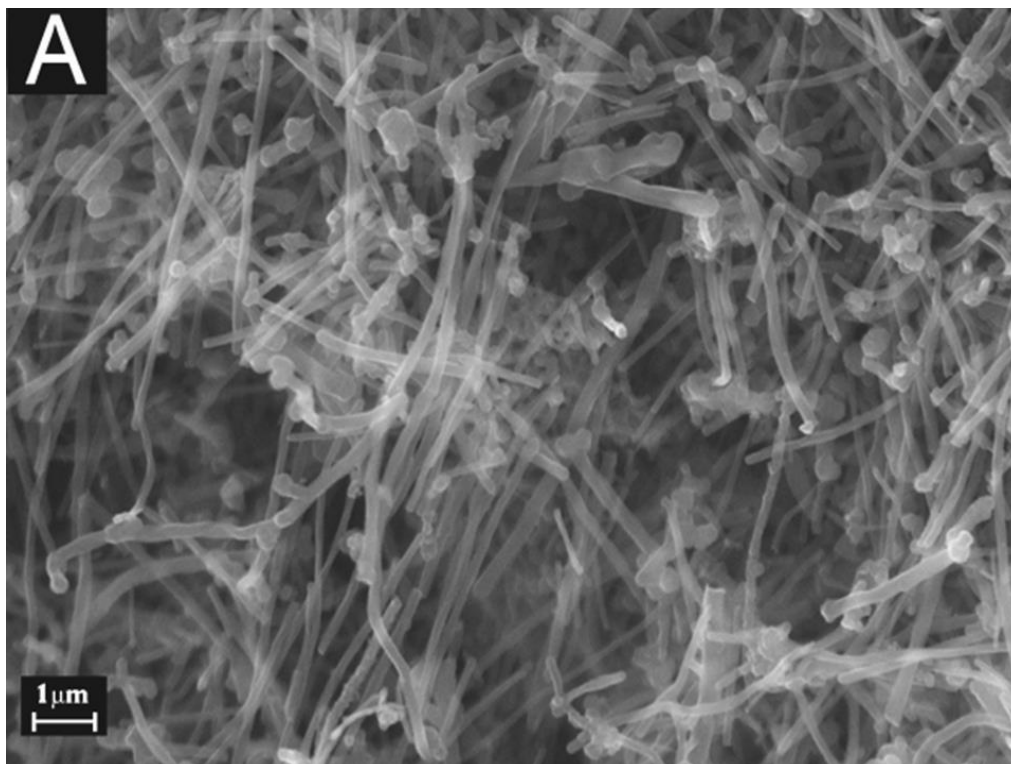


Figure 2. Cesarino, I. et al.

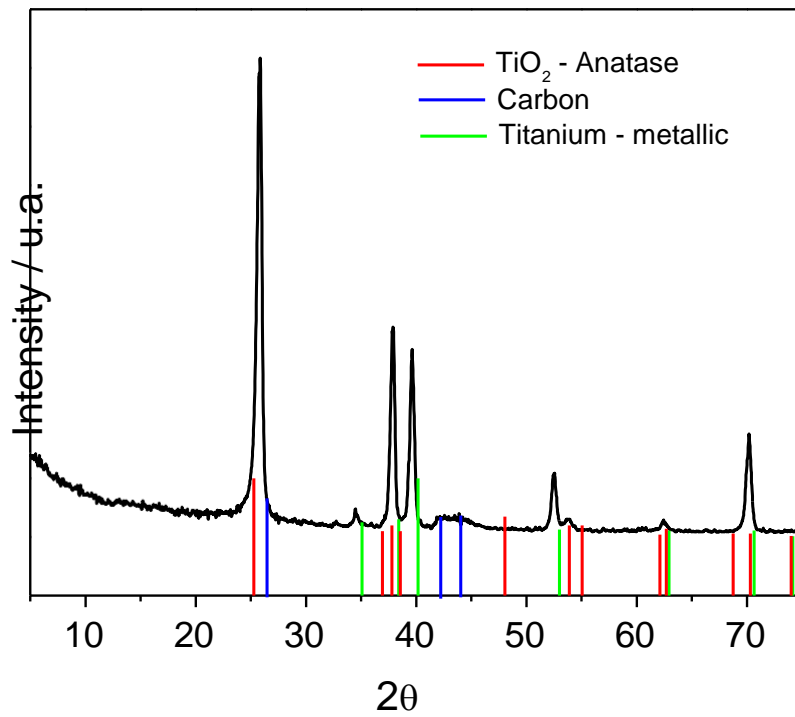


Figure 3. Cesarino, I. et al.

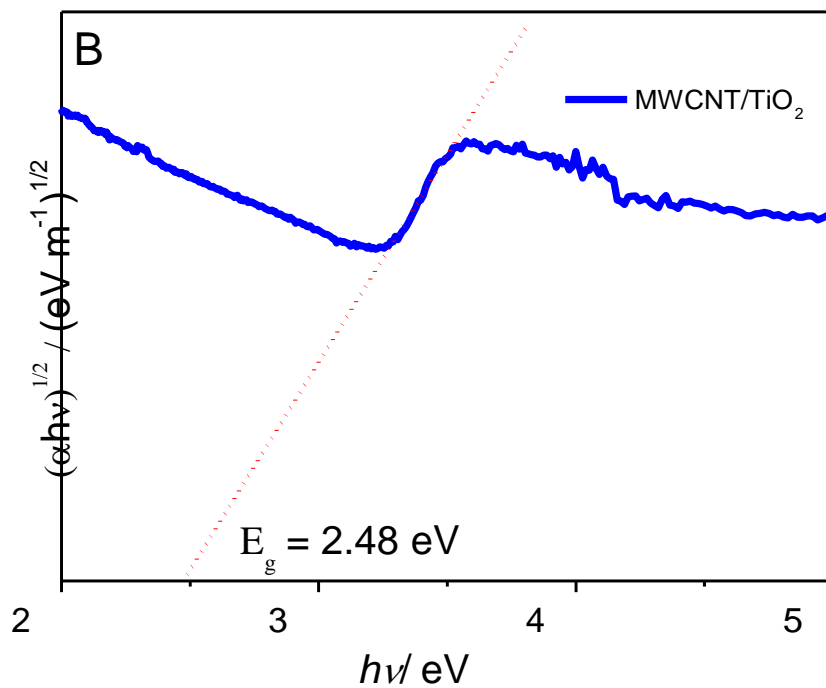
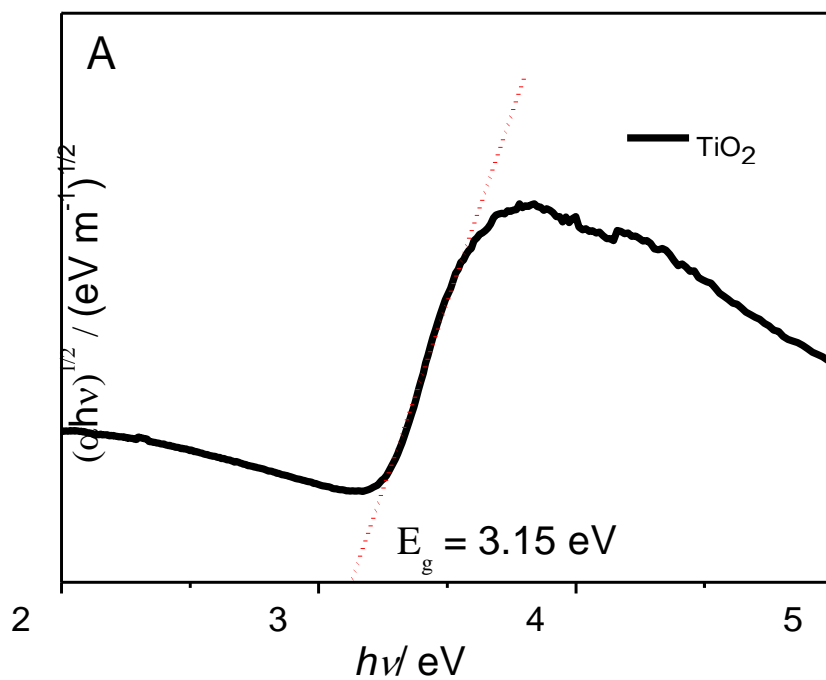


Figure 4. Cesarino, I. et al.

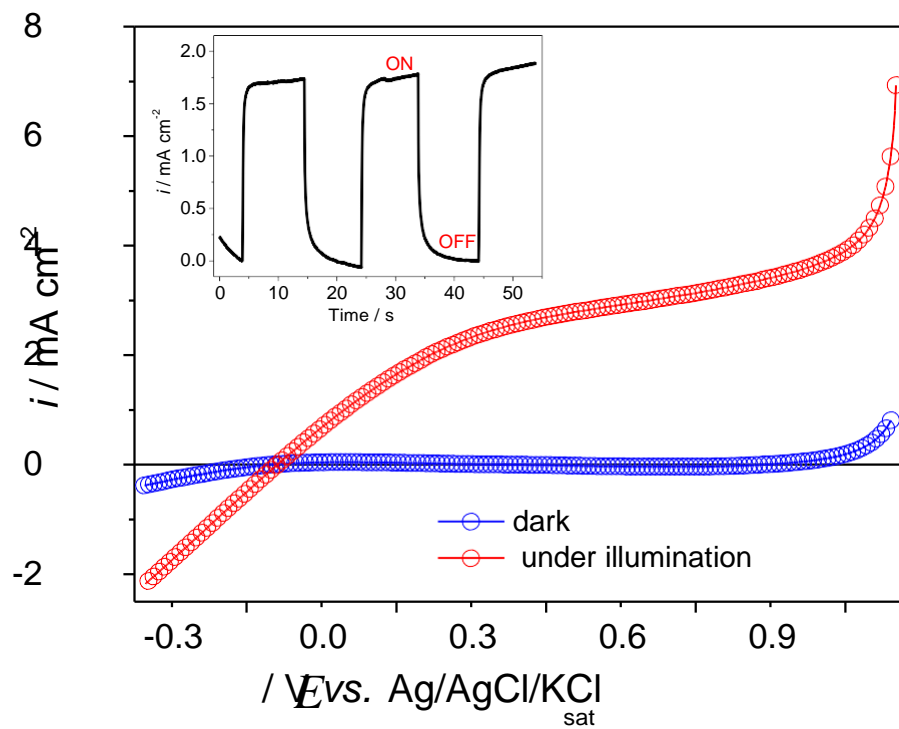


Figure 5. Cesarino, I. et al.

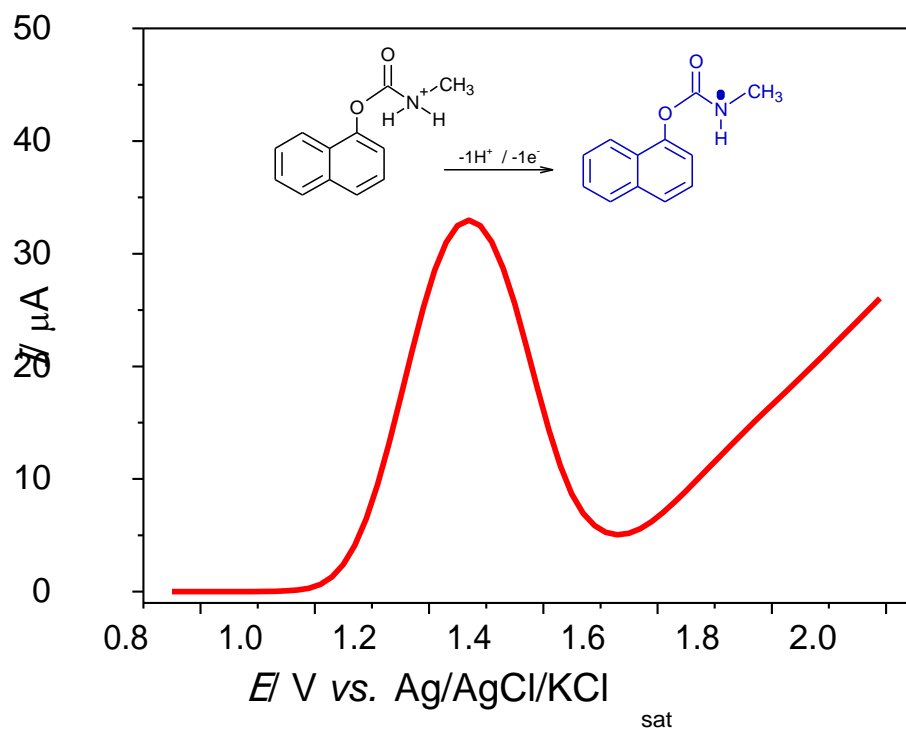


Figure 6. Cesarino, I. et al.

